Journal of Materials Science Research and Reviews

Volume 6, Issue 4, Page 655-669, 2023; Article no.JMSRR.105081

Water Release Kinetics of Hygroscopic Acrylamide Enbibed in $CaCl_2$ by Thermogravimetric and Differential Scanning Calorimetry Methods

Nasrollah Hamidi [a*] and Mehrdad Yazadani-Pedram [b]

[a] Department of Biological and Physical Sciences/1890-Research, South Carolina State University, Orangeburg, SC 29117, USA.
[b] Facultad de Ciencias Quirnicas y Farmaceuticas, Universidad de Chile, Santiago, Chile.

Authors' contributions

This work was carried out in collaboration between both authors. Both authors read and approved the final manuscript.

Article Information

Open Peer Review History:
This journal follows the Advanced Open Peer Review policy. Identity of the Reviewers, Editor(s) and additional Reviewers, peer review comments, different versions of the manuscript, comments of the editors, etc are available here: https://www.sdiarticle5.com/review-history/105081

Original Research Article

Received: 11/06/2023
Accepted: 19/08/2023
Published: 01/09/2023

ABSTRACT

Hygroscopic thermo-responsive materials, such as poly(acrylamide) gel (PAAG), are appropriate candidates for building atmospheric water generators (AWGs) to address freshwater stresses for innovative industrial endeavors. The PAAG has been synthesized by radical polymerization of acrylamide and N,N'-methylenebisacrylamide in the presence of carbon nanotubes. The dry gel was embedded with calcium chloride to produce a deliquescent acrylamide hydrogel (DHG) capable of capturing environment vapor by 20% of its mass per day. Its highest water release rate was at temperatures close to 45 °C, the temperatures that can be achieved through the photothermal effect of sunlight. The $\mathbf{E_a}$ of DHG to release water has been found to be about 46 $kJmole^{-1}$, which is close to the vaporization energy of water. The highest water release rate was closed to 45 °C, at the heating rate of 0.50 $Kmin^{-1}$, and moved to a higher temperature as the heating rate increased due to the thermal lag effects. The DSC thermogram showed a transition

**Corresponding author: Email: Nhamidi@scsu.edu;*

centered around 50 °C, which coincides with TGA's maximum water release rate. This indicates that the release of water by DHG was due to its phase transition from hydrophilic to hydrophobic, a phenomenon that also has been confirmed by other researchers.

Keywords: Hydrogel; dew collection; freshwater; desiccants; thermo-responsive gel; kinetics triplet.

1. INTRODUCTION

This work reports the preparation and process of absorption and desorption of a sample of a poly(acrylamide) hydrogel embedded in $CaCl_2$ and immersed in carbon nanotubes by thermogravimetric analysis (TGA) and differential scanning calorimetry (DSC). Other researchers have studied the hydrogel [1,2] and considered it as an effective agent for harvesting environmental water and fabricating AWGs [3,4]. The maximum rate of water release was estimated at each thermogram by its derivative with respect to time. The TGA thermograms and their derivatives were analyzed based on the isoconversional method to estimate the kinetics triplet for water desorption at the temperature range of 30-120 °C. The obtained values were within expectations and supported the funding in the published literature.

Earth overflows with 1,386 million cubic kilometers of water; only 35.5 million cubic kilometers (2.5%) is freshwater. Less than 0.75% of this freshwater is sustainably managed. Human activities and climatic changes are causing freshwater resources to decline, leading to water anxiety as the 5th global risk [5-10]. Worldwide, potable water accelerated consumption continues to increase thrice within the last 50 years [7,11,12]. Foods production withdraws over 74% of water, and a 14% increase was predicted by 2030 [13-15]. Moreover, mineral contamination is a fundamental problem in many places, such as 50 countries living in the Pacific Ring of Fire [16]. Desalination of seawater and inland saline water [17,18], could alleviate water stress for more than 4 billion people [19] who live near saline regions [15,20]. The availability of individual AGW units working with the force of nature would alleviate many water-stressed situations. The freshwater stress would alleviate far and wide by harvesting the renewable, invisible atmospheric vapor, which is estimated to be equivalent to 12,900 cubic kilometers of liquid water, by developing "atmospheric water generators" (AWGs) [21,22]. In some arid and humid areas of Asia, America, and Africa, AWGs collecting fog, rain, and vapor have been installed to alleviate local water stress and prevent forced relocation and poverty [23-25].

The amount of steam (~ 1-3%, depending on location) [26] is measured as the percent of relative humidity (% RH), and its concentration depends on the location, time, temperature, geographic and climatic conditions [22,27]. A warmer atmosphere holds more moisture - about 7 percent more per one (1°C) of warming- than a colder one. Temperature variations during day and night cause changes in the water content of air, leading to dewfall as a natural water source for plants and animals, particularly in arid and humid regions. Also, it is used for human consumption as AWGs become more popular [28]. Active AWGs require a significant energy input resulting in a substantial heat release, and their mechanism is more thermodynamically complicated than passive AWGs and fog harvesters [3,29-32].

The emergence of temperature-responsive polymers that regulate water condensation and release at the molecular level by transitioning from hydrophilic to hydrophobic by temperature changes has increased the success of AWGs fabrication. When they are planted in an interpenetrating polymeric gel network, they capture moisture from the air at lower temperatures and release water by a phase separation process at a slightly higher temperature. Poly(acrylamide) [3], poly(N-vinyl caprolactone) [33], poly(N,N-diethylamino ethyl methacrylate), poly(pyrrole chloride) (PPy-Cl) [34], poly(N-isopropylacrylamide) (PNIPAM) [35,36] and some copolymers such as poly(L-lactic acid)−poly-(ethylene glycol)−poly(L-lactic acid) are among those stimuli-responsive polymers [36-38]. This behavior has led to the creation of responsive nanostructured polymer materials and systems in the form of thin films, particulates, and assemblies to harvest environmental water. Smart materials by themselves and in a network of hygroscopic minerals and polymers have provided a good moisture absorption and desorption network [39-41]. The hydrogel becomes hygroscopic [42] by adding sorbents such as salts,[3] metal−organic framework,[43] or hygroscopic polymers [44].

Generally, three processes co-occur inside the hydrogel: [45] vapor transport, sorption, and liquid transport. Vapor transport through the interconnected gaseous micropores relies on diffusion due to the presence of a vapor pressure difference. Sorption occurs on the liquid−gas interface of the micropores. Meanwhile, the liquid is transported through the nanopores of the polymer network, driven by the water chemical potential difference between the wet and dry regions of the polymer network [46]. The redistribution of water leads to the structural change of micropores and polymer networks and further induces a volumetric expansion of the hydrogel due to the pore elastic effect [47]. This effect, in particular, is unique to hydrogels compared to other commonly used sorbent systems with rigid materials [26].

PNIPAM undergoes a phase transition at its LCST near 32°C [35,36]. Hair-size fibers made of a mixture of hydrophobic plastics with hydrophilic PNIPAM were capturing water from a highly humid atmosphere at lower temperatures (below 25°C) within a few minutes and released it at above 35°C [35]. The amounts of thermo-responsive PNIPAM at the skin layer controlled the wettability of the fibers. Other hydrophilic polymers, such as nylon, have also given good results when electro-spared on the surface of the fibers. Also, a combination of PNIPAM with hydrophilic sodium alginate made an interpenetrating polymer network gel that can capture moisture from the air and directly extract liquid water [24,36,38,39].

Metal-organic frameworks (MOFs) resulting from reticular chemistry are another kind of three-dimensional interconnected network of highly porous crystalline solid materials suitable for AWGs fabrication [26,40,41]. The desorption process requires heat input depending on the water molecules' adsorption strength to reach regeneration temperature, which varies from 70 - 170°C [31,48].

Hygroscopic minerals such as calcium chloride, lithium chloride, lithium bromide, silica gel, and zeolite attract moisture everywhere in very low and highly humid environments [24,49-53]. These moisture absorbents have been used to fabricate AWGs that harvest moisture at night when the worm air gets cold and its humidity increases. The water desorption occurred during the day by heating the hygroscopic bed with solar radiation in a closed container [24]. For example, in a dry and arid region experiencing a 20% RH at 30°C, an energy-intensive and impractical process must cool the air to below its dew point (~ < 4°C) to turn vapor into dew. However, by heating the humid descants in a closed container, air humidity reaches above 80% RH at 30 °C in the cabin, then the vapor liquefied at temperatures below the dew point (below 26°C). This process requires less energy than extracting water from dry and arid environments [54-56].

2. EXPERIMENTAL

2.1 Materials

Carbon nanotubes (CNTs), nitric acid, sulfuric acid, acrylamide (AA), N, N'-methylene bis acrylamide (MBAA), and benzyl peroxide were purchased from Fisher Scientific, a Thermo Fischer Scientific (USA) company. They have been used as received. Fresh distilled water was prepared in the lab.

2.2 Synthesis

5 mL of distilled water, 1 g of acrylamide (AA), 0.85 mg of N, N'-methylene-bis-acrylamide (MBAA) as a crosslinking agent, 0.56 mg benzyl peroxide as the polymerization initiator, 220 mg CNT as solar heat absorbent has been added to a 60 mL Thermo-Scientific™ screwed cap septum vials. The mixture has been held for 30 min under a stream of 30 $mLmin^{-1}$ ultrapure argon to eliminate the oxygen present, then held in an ultrasound bath for 2 hours and let settle overnight on top of a hot plate at ~70°C. The product was AA hydrogel with little CNTs inside of it. The sample was freeze-dried for 24 hours and then immersed in a 1 M solution of $CaCl_2$ for 24 hours under laboratory conditions. The saturated hydrogel has been dried in an oven at 60°C for a week. Water absorption of DHG in the outside environment and its desorption by sunlight have been not studied.

2.2.1 Instrumentation

2.2.1.1 Thermogravimetric analysis (TGA)

The TGA studies have been conducted on a TGA-7 Thermogravimetric Analyzer (PerkinElmer, Inc., USA) run on a Dell PC using Pyrus 13.2.3. It was calibrated with four points calibration method since the thermocouple in this device is not in direct contact with the sample. The absorption reaction has been prevented by increasing temperature linearly and a well-

controlled nitrogen stream of 60 $mLmin^{-1}$ (room temperature and atmospheric pressure), which carried the volatiles away as soon as they formed. The sample weight preserved was recorded continuously with the corresponding temperature and time. Several scans were carried out at the rates of 0.5, 1, 2, and 5 $Kmin^{-1}$ to evaluate the kinetics parameters accurately. After each scan, the sample was exposed to the lab environment for a few days to saturate with vapor. The data were downloaded to Microsoft Excel for the study. The values of the extent of desorption (α) for each sample were estimated by $\frac{(\%W1-\%Wi)}{(\%W1-\%Wf)}$ where %W1 represents the initial weight percent of the sample, usually 100%, %Wi represents the normalized weight of the remaining sample at any time, and %Wf represents the %W of the sample at the end of the dehydration process. The values of α increased from zero to one as the dehydration progressed from initiation to completion, respectively.

2.2.1.2 Differential Scanning Calorimetry (DSC)

The DSC experiments were carried out on a DSC-7 Differential Scanning Calorimeter (PerkinElmer, Inc., USA) under a stream of 60 $mLmin^{-1}$ of argon, operated by a Dell PC using Pyrus 13.2.3. The instrument was calibrated using a standard sample of indium. A well-dried DHG aliquot in a mortar and pestle was crashed and blended before inserting it into an aluminum DSC pan for thermal analysis.

3. RESULTS AND DISCUSSION

3.1 Water Sorption Experiments

About 1 g of the DHG generated earlier was placed on a Mettler-Toledo Balance (28 °C, 57% RH during July 2022, in Hodge Hall Lab 314) to monitor its water absorption capacity by its weight increase for three days, as shown in Fig. 1. The over 20% of weight increase of DHG is an indication of its ability to absorb environment moisture within 7.5 hours (h), 50% of its weight after 28 h, and over 60% of its original weight when exposed for 50 hours to the lab environment. The rate of moisture absorption by hydrogel decreased over time; the initial moisture absorption rate was 0.042 $\%min^{-1}$. The rate of environmental water absorption became slower on the second day (0.022 $\%min^{-1}$), and much slower on the third day (0.012 $\%min^{-1}$) of exposure to the air, s was expected.

3.1.1 Photo-thermal bath

To compare the TGA situation with the outside environment, charcoal was taken as an example of photothermal absorbent material assuming its photo absorption is similar to the CNTs. The temperature increase of the charcoal was monitored every 5 mins interval, using an

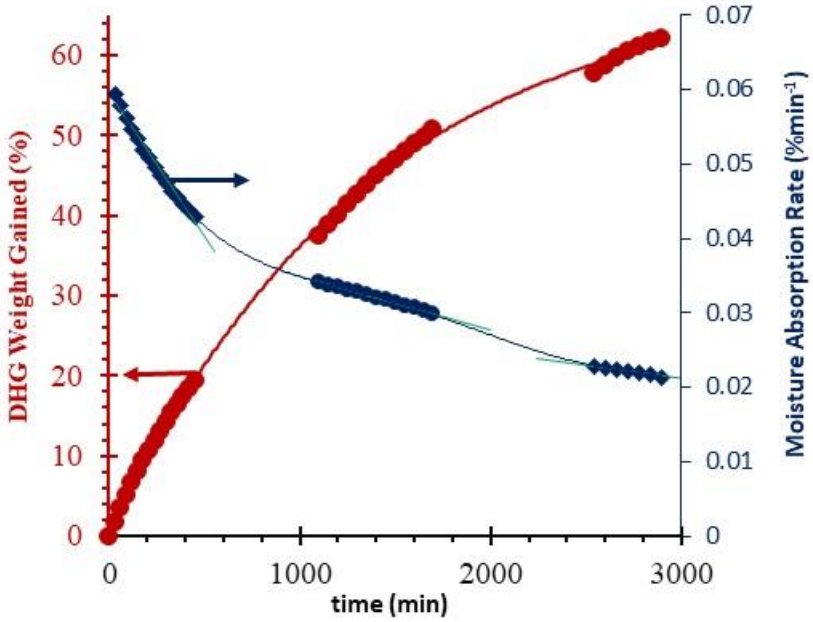

Fig. 1. DHG moisture absorption and its rate

infrared thermometer, from 10 AM to 1 PM on a sunny day (June 2022) when the highest daily temperature was 36°C. The charcoal absorbed solar heat at a very high rate at the beginning. After 50 min, the temperature changes plateaued, as shown by the graph in Fig. 2.

3.1.2 Differential scanning calorimetry (DSC)

Some industrial applications and the materials' processing types relate to the physical properties of matter, such as melting point (mp) and glass transition temperature (Tg). The relatively high mp (> 300°C) and Tg temperatures (~163°C) of polyacrylamide (PAA) result from strong polar interactions between polar amide groups. During the first DSC scan of the DHG as shown in Fig. 3, its physical changes have been registered at temperatures ~ 50.°C (ΔH ~ 22.7 Jg^{-1}), and 179 (ΔH ~ 371 Jg^{-1}). These transitions do not coincide with mp (> 300 °C) and Tg (~163°C) of PAA. Also, they are not related to the AA's mp (84.5°C). Therefore, they are related to the new product DHG, as has been expected. The same transition was reproduced at 48°C (ΔH = 77 kJ/g when the sample was scanned again (2° Run) 3 days later.

The transition that started around 35°C and maximized around 50°C could be related to a phase transition and conformational rearrangements of DHG. This thermal transition could also be responsible for the spontaneous release of absorbed vapor in the form of liquid water at temperatures above 40°C as has been supported by other researchers' work.

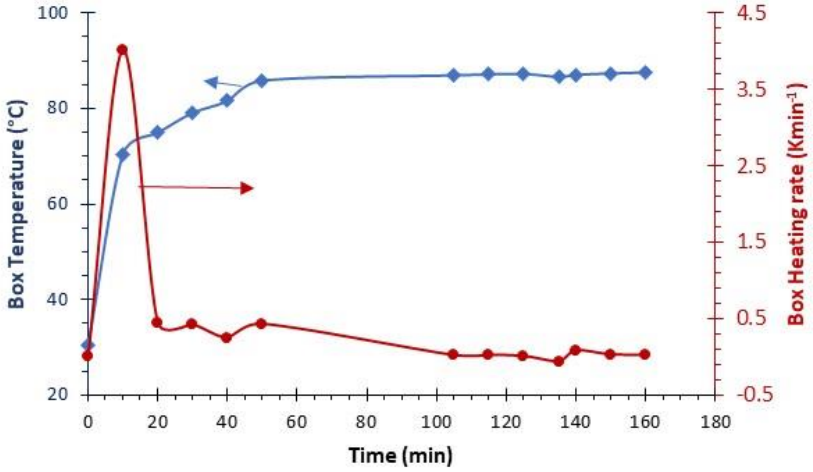

Fig. 2. Aluminum charcoal box temperatures under direct sunlight

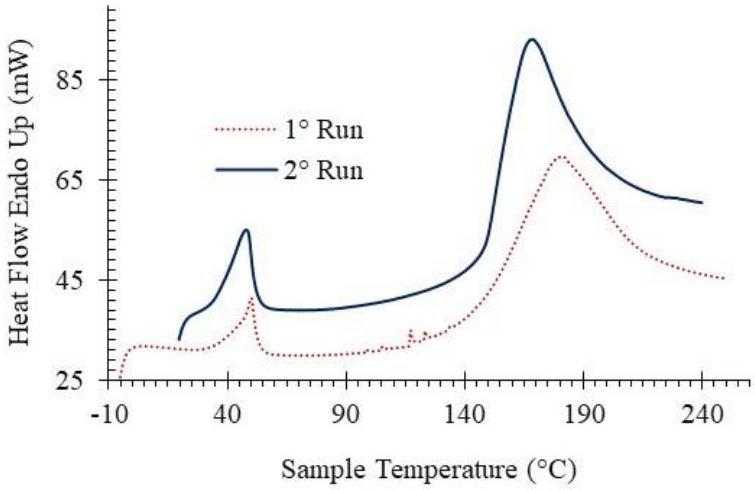

Fig. 3. Thermogram of differential scanning calorimetry (DSC) of a sample (27.73 mg) of DHG at the β = 10 $Kmin^{-1}$

3.1.3 Thermogravimetry studies

A TGA pan was loaded with 32 mg of dry hydrogel for water desorption analysis. The sample was held at room condition for five or more days to absorb humidity before each thermal scan. The weight loss by temperature and time was taken as the measure of water desorption by DHG. The variations of normalized weights (%W), advancement of water release (α), and its normalized rates are shown by the graphs in the plots of Fig. 4 (a), (b), and (c), respectively. At the slower heating rate, β = 0.5 Kmin^{-1}, the DHG released about 72% of the absorbed water at temperatures below 60°C as shown by the corresponding graph in Fig. 4 (a).

The water desorption was initiated as soon as the sample was placed into the TGA pan (~ 27°C), The yield of water released at a given temperature depended on the heating rates, as can be observed with the data listed in Table 1. As the heating rate increased, less water was desorbed at lower temperatures, indicating the importance of the factor of time on water desorption and thermal lag on the sample. Time requires to transfer energy from the furnace to the sample. In this case, the higher heating rate has less effectiveness.

The tendency of the variation of α and normalized rate of dehydration by temperature in Fig. 4 (b) have the shape of a sigmoid reaction, where the rate of dehydration at the starting point is zero, it increases by the advancement of the dehydration, reaches to a maximum and then decreases.

The maximum rate of water desorption (R_{max}) also depended on the heating rate, as shown in Fig. 4 (c) and the data listed in Table 2. The maximum rate of water yield was at temperatures below the boiling point of water, ranging from 47 to 79 °C for the $\beta \leq 2$ Kmin^{-1}; and over 106°C for the β = 5 Kmin^{-1}. Our results were within expectations since other researchers also reported the release of water from acrylamide gels at very low temperatures achievable by photothermal CNTs [3]. At the β = 0.5 Kmin^{-1}, the R_{max} was achievable at t > 45; however, it was smaller than the rates at the other βs values. At higher β, the rates of water release are larger, but their maximum shifts to higher temperatures (Table 2), which is an indication of more energy requirement to harvest water.

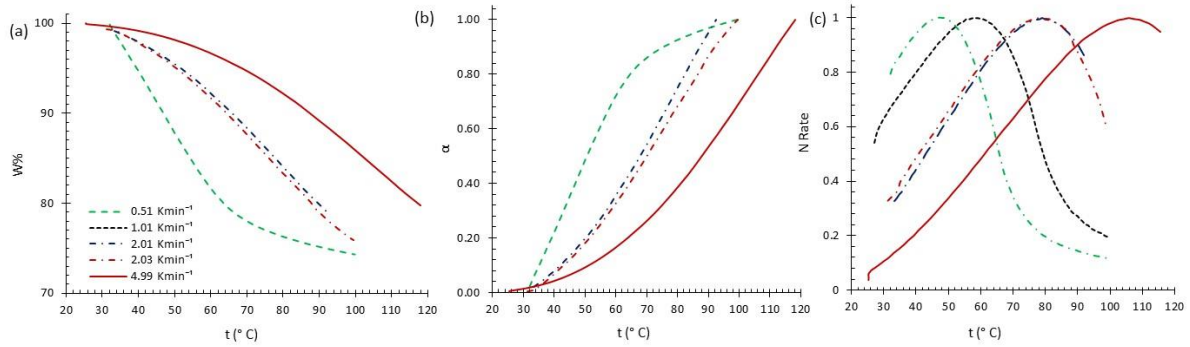

Fig. 4. (a) Thermograms of water desorption, (b) Water desorption advancement, and (c) normalized water desorption rate of the DHG studied by TGA

Table 1. The amount of water yields in the temperature range 40 to 90°C by heating rates ranging from 0.5 to 5 Kmin^{-1}

β (Kmin^{-1})	%Water yield at temperature (°C)					
	40°	50°	60°	70°	80°	90°
0.5	5.2	12.3	18.4	22.1	23.8	24.9
1.0	5.0	9.6	14.4	19.3	22.4	24.1
2.0	3.5	4.5	7.8	11.8	16.3	20.2
2.0	2.1	4.8	8.1	12.4	16.7	20.9
5.0	0.8	1.9	3.2	5.1	7.8	10.7

Table 2. The thermograms parameters at the maximum rate of water yield

β (Kmin^{-1})	R_{max} (%min^{-1})	T_{max} (°C)	α	Water yield (%)
0.5	0.347	47	0.413	10.3
1.0	0.259	58	0.539	13.6
2.0	0.901	79	0.729	15.5
2.0	0.922	78		15.9
5.0	1.78	106	0.795	16.1

3.1.4 Kinetics of water desorption

The kinetics of hydrogel desorption is distinct due to the presence of gas, liquid, and polymer network.

The kinetics of the thermally simulated dehydration of the DHG was studied by the measurement and parameterization of the rates of weight loss originating by eq.1: [57].

$$\text{DHG (active)} \xrightarrow{\Delta} \text{DHG} + H_2O\ \text{(vapor)} \quad (1)$$

Moist DHG(active) was heated ($\xrightarrow{\Delta}$) to released absorbed humidity in the form of vapor [H_2O (vapor)] or nano-droplets of water that were carried away with the stream of nitrogen (wind). The rate of thermally stimulated dehydration of DHG (-dW/dt) is expressed by the negative derivative of TGA thermogram (-DTGA). The rate of dehydration is parameterized by the advancement of dehydration (α) where (1-α) represents the residual amount of DHG(active) or residual remaining water in the sample, the mechanism of the water release expressed by *f*(α) function (Table 3), and the Arrhenius rate constant [k(T)], as shown by eq. 2: [58,59].

$$\text{Rate} = \frac{d(1-\alpha)}{dt} = -k(T).f(\alpha) = -f(\alpha).A.\text{Exp}(-\frac{E_a}{RT}) \quad (2)$$

where T represents the absolute temperature value in K, $\mathbf{E_a}$ represents the energy barer to release water by the DHG, and R = 8.314 J mol^{-1} K^{-1} is the universal gas constant. Equation (2) is the starting point for various differential kinetic methods and applies to any reaction type. The values of $\mathbf{E_a}$, and ln**A**, with the pre-assumed form of *f*(α) are estimated from the slope and intercept of the Arrhenius plot based on eq. 3, [lnRate/*f*(α)] = ln k versus 1/T, for a given value of α, as shown in Fig. 5.

$$\ln\left[-\frac{dw/dt}{f(\alpha)}\right] = \ln k = \ln\left[\frac{\frac{d\alpha}{dt}}{f(\alpha)}\right] = -\frac{\mathbf{E_a}}{RT} + \ln\mathbf{A} \quad (3)$$

Eq 3 applies to the TGA data since it provides the weight, temperature, and rate of weight lost at each interval. The pre-assumed models, *f*(α) values used in this work are shown in Table 3.

Table 3. Pre-assumed reaction models are used to describe the thermally stimulated water release of the DHG system

No.	Reaction Model	Code	*f*(*α*)
1	Power law	P4	$4\alpha^{3/4}$
2	Power law	P3	$3\alpha^{2/3}$
3	Power law	P2	$2\alpha^{1/2}$
4	Power law	P2/3	$2/3\alpha^{-1/2}$
5	One-dimensional diffusion	D1	$1/2\alpha^{-1}$
6	Mampel (first order)	F1	(1 – α)
7	Avrami–Erofeev	A4	$4(1-\alpha)[-\ln(1-\alpha)]^{3/4}$
8	Avrami–Erofeev	A3	$3(1-\alpha)[-\ln(1-\alpha)]^{2/3}$
9	Avrami–Erofeev	A2	$2(1-\alpha)[-\ln(1-\alpha)]^{1/2}$
10	Three-dimensional diffusion	D3	$3/2(1-\alpha)^{2/3}[1-(1-\alpha)^{1/3}]^{-1}$
11	Contracting sphere	R3	$3(1-\alpha)^{2/3}$
12	Contracting cylinder	R2	$2(1-\alpha)^{1/2}$
13	Two-dimensional diffusion	D2	$[-\ln(1-\alpha)]^{-1}$
14	Random Scission	L2	$2(\alpha^{1/2}-\alpha)$

The isoconversional method assumes that the mechanism of a reaction remains the same at a given α value, independent of the heating rate. It was used to construct the Arrhenius plot for the given α values of the DHG, as shown by the plots in Fig. 5. The slope of the list-squarer adjusted line to the data represents the value of $\mathbf{E_a}$/R. A negative slope of the adjusted lines to the experimental data represents an endothermic $\mathbf{E_a}$, as was expected.

Fig. 6 (a) shows the variation of the energy barrier values ($\mathbf{E_{a,\alpha}}$) obtained by applying the isoconversional method (Eq 3), for the values of α ranging from 0.05 to 0.95 using the reaction models enlisted in Table 3. The corresponding values of ln**A** are shown in Fig. 6 (b), while their $\mathbf{r^2}$ values are shown in Fig. 7. For a given value of α, the estimated values of $\mathbf{E_{a,\alpha}}$ from the slopes of the list-square adjusted lines were close to each other, independent of the *f*(α) function, as shown by the concentric points in Fig. 6 (a), and was expected from requirements of the method. For instance, the average values of the $\mathbf{E_{a,\alpha}}$ obtained from the slope of all models for $\boldsymbol{\alpha}$ = 0.300 was $\mathbf{E_{a,\ 0.300}}$ = 46.44 ±0.01 kJmol^{-1} with the corresponding ln$\mathbf{A_\alpha}$ = 16.0 ± 0.7 min^{-1} and for α = 0.700, the $\mathbf{E_{a,\ 0.700}}$ = 46.16 ± 0.01 kJmol^{-1}, with the corresponding ln$\mathbf{A_\alpha}$ = 15.6 ± 0.6 min^{-1}. The relative constancy of the values of $\mathbf{E_{a,\alpha}}$ = 47 ± 1 was observed for 0.2 < α < 0.8. The values of $\mathbf{E_{a,\alpha}}$ outside of the mentioned boundaries were larger due to the higher energy amount needed to release water. Similar tendencies of constant values were observed for ln$\mathbf{A_\alpha}$ 15.9 ± 0.4; though, these values were scattered as shown in Fig. 6(b). As was expected, the high value of the standard deviation related to ln$\mathbf{A}_\alpha$ is due to the chosen reaction model, the *f*(α) function. The values of ln$\mathbf{A_\alpha}$ outside of the mentioned boundaries also were larger than the inside, having a similar trend as $\mathbf{E_{a,\alpha}}$, as was expected.

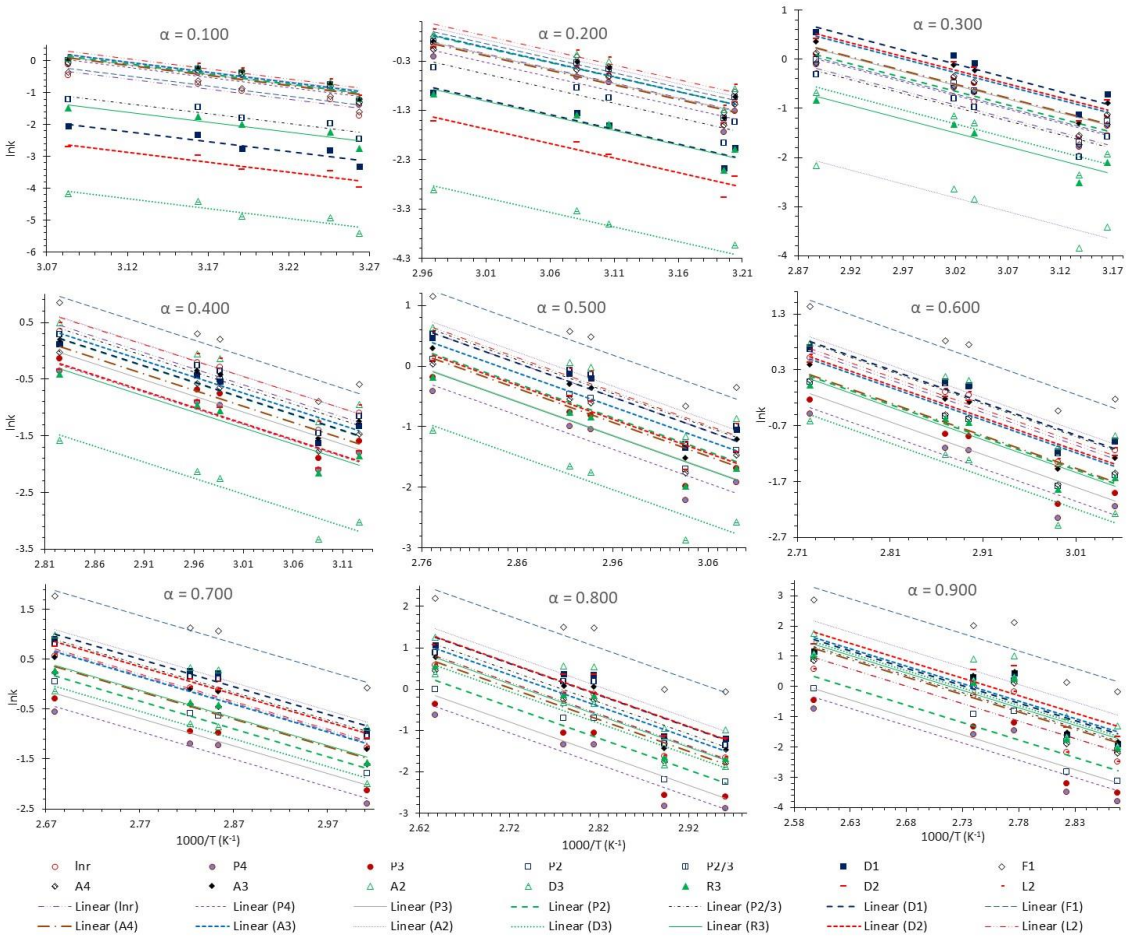

Fig. 5. Arrhenius plots of the DHG dehydration at the indicated α values

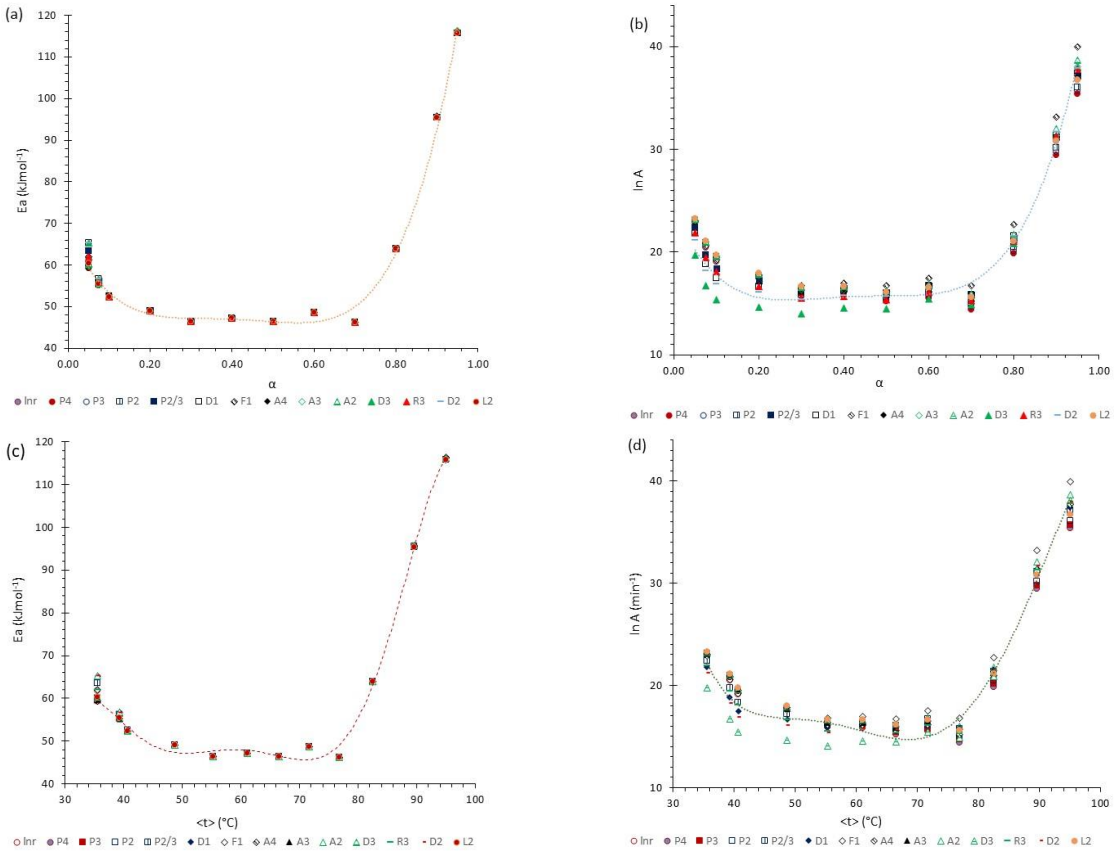

Fig. 6. Variation of (a) activation energy barrier ($E_{a,\alpha}$) and (b) values of Arrhenius pre-exponential factor (lnA) of dehydration of DHG versus the corresponding extent of reaction (α); and the variation of (c) $E_{a,\alpha}$ and (d) lnA_α of DHG versus the corresponding average temperature <t>

According to Eq. 3, there is an interdependency between the values of E_a and lnA. This interdependency has been confirmed by comparing Figs. 6 (a) and (b) where they show that both $E_{a,\alpha}$ and lnA_α have approximately a similar trend (disregarding the ln A_α scattering). These "effective", "apparent", "empirical", or "global" values of $E_{a,\alpha}$ and lnA_α, most likely, are composite values, determined by the sum of kinetic parameters of the involved individual steps assuming that the water delivery has the Arrhenius temperature dependency [57,60]. Global kinetic parameters differ from intrinsic parameters; they can vary strongly with the temperature and the extent of conversion [60-62] or take on negative values [63]. Such discrepancies are not expected for the $\mathbf{E_a}$ values of a single-step chemical reaction or a simple physical change. The relative constant values of kinetic parameters at the extent of $0.2 < \alpha < 0.8$ are an indication of a single change, vaporization of water since average values of $\langle E_a \rangle = 47 \pm 1$ kJmol^{-1} in the range of $0.2 > \alpha > 0.8$ as illustrated by E_a versus α, in Fig. 6 (a) is comparable to the values of the heat vaporization of water at saturated vapor pressure (~ 45 kJmol^{-1}). Therefore, the E_a obtained in this work is related to the vaporization of water during the experiment. As the heating rate was slower, the sample had time to gain the energy needed for the process. This fact also can be deduced by the data listed in Tables 1, and 2.

The approach to evaluating independently $\mathbf{A_\alpha}$ and $f(\alpha)$ in a model-free method was explained in detail by other authors [64-66]. These studies emphasized correlations between the reaction rate and activation energy, and pre-exponential factors of the individual steps of a chemical reaction, and changes in the rate-limiting steps. Since the rate of reaction ($d\alpha/dt = \mathbf{R_\alpha}$) at a given α value is expressed as the product of two terms, [$\mathbf{A_\alpha}$ $f(\alpha)$] and [$\exp(-\mathbf{E_\alpha}/RT)$], therefore, as the value of $\mathbf{R_\alpha}$ decreases, and one of the two terms increases the other decreases. When the term of $\mathbf{E_\alpha}$ becomes dominant, it is a sign of a change in

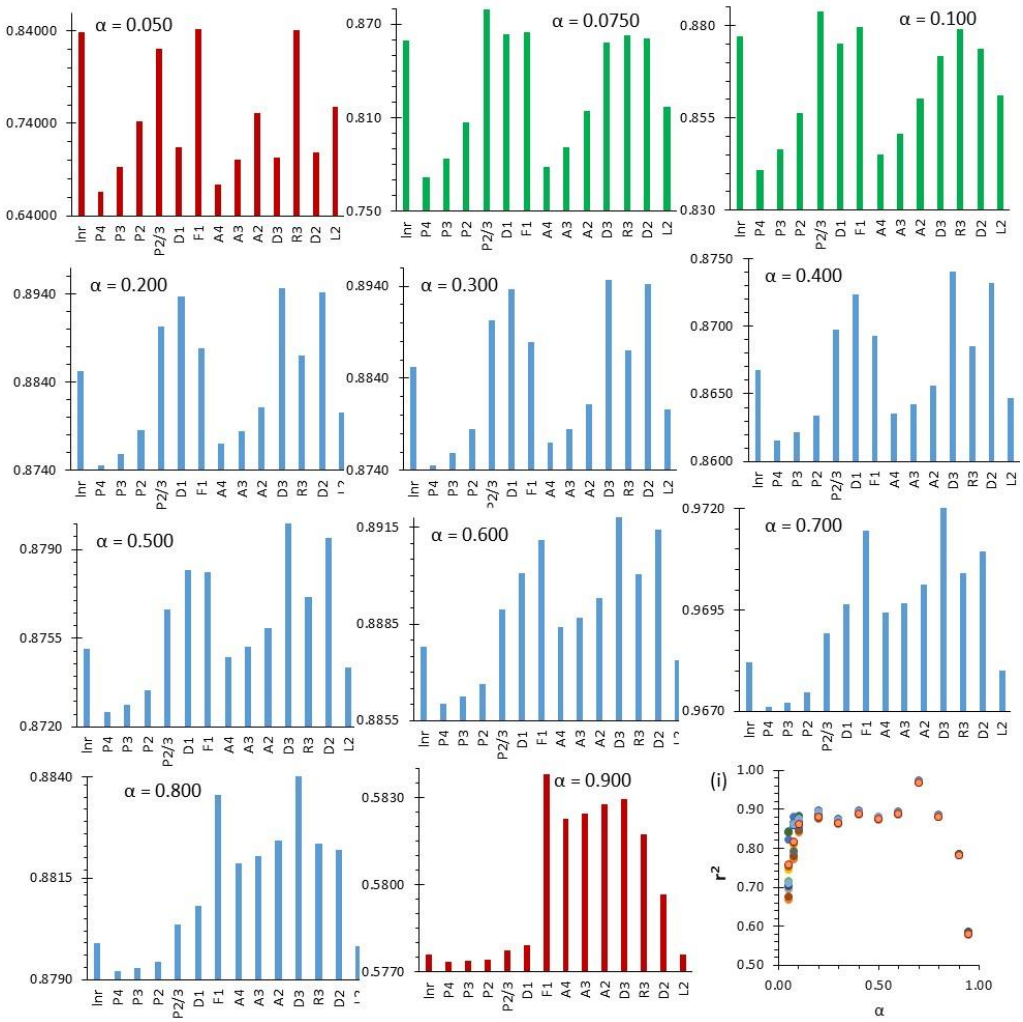

Fig. 7. Comparison of the values of r^2 of each *f*(α) (Table 3) at the indicated values of α; and (i) variation of r^2 versus

the limiting step of the reaction. At the values of α > 0.8, the values of $\mathbf{E_a}$ increased by increasing values of α, as shown in Fig. 6 (a). The increase of $\mathbf{E_a}$ in the plot by increased α values is due to reducing the amounts of easy accessed water generated by the phase transition of the PAA gel.

The isoconversional method assumes that the mechanism of a reaction at a given extent of reaction is independent of the heating rate in TGA thermogram, and hence independent of temperature. Therefore, the same reaction, in each α value, is taking place at various temperatures, depending on the heating rate due to thermal lag, as it is illustrated by Arrhenius plots in Fig. 5. We assume that the average temperature of a given α value would represent the temperature for the reaction at that particular α, and it is shown by <t>. The variation of $\mathbf{E_{a,\alpha}}$ and $\ln A_\alpha$ versus <t> are illustrated in Fig. 6 (c) and (d), respectively. Comparing Figs. 6 (a) (c) illustrate a similar tendency of variation of energy by α and <t>, respectively. Therefore, the approach could be considered valid.

The values of $\mathbf{E_{a,\alpha}}$ of the DHG sample decreased by increasing the values of α and temperature and reached to its lower values in α > 0.2 > 0.8 where temperatures ranging from ~40 to 77°C, as illustrated by Fig 6 (c). At < t > higher than 80°C, the values of $\mathbf{E_{a,\alpha}}$ increase by increasing temperature to the end of the dehydration process, as shown in Fig. 6 (c). Lowering energy barrier of dehydration of polyacrylamide gel by temperatures 40s°C values made the DHG be an appropriate candidate for spontaneous moisture absorbance from the environment at temperatures below 40°C and release it at

temperatures above 40°C. The increase of $\mathbf{E_a}$ in the plot by increased temperatures is due to reducing the amounts of easy arresting water due to phase transition of DHG from hydrophilic to hydrophobic. The lowest value of $\mathbf{E_a}$ to release water was around 46 kJmol^{-1} at 50°C; it is easily achievable by photothermal embedded in the gel. In this case, as soon as DHG released its water, the water was moved out by the stream of nitrogen. Moreover, at temperatures above 80°C, the amounts of $\mathbf{E_{a,\alpha}}$ are increasing by increasing the temperature, indicating the consumption of the DHG easier release water at lower temperatures due to the phase transition of the polymer gel as shown by DSC (Fig. 3) which causes the released of stored water spontaneously. The remaining water bonded strongly to DHG and its extraction requires more energy.

The values of the pre-exponential factor (ln**A**) of DHG are in the range of (1.74-318) X 10^5 Hz with the highest values at the beginning and end of the dehydration, as shown in Fig 6 (b). The values of the standard deviation of **A** were smaller at the middle indicating a single change, and larger at the beginning and end of dehydration resulting from multiple changes in the system. The lowest values of **A** belonged to Model D3, as well the best fitting correlation expressed in the highest values of r^2 as shown in Fig. 7.

4. CONCLUSIONS

The water release of DHG was analyzed based on the kinetics of a pseudo-single-component overall models (PSOM) decomposition reaction. Fig. 7 compares the variation of the values of the best fitting (r^2) model of the pre-assumed $f(\alpha)$, for each α value. The first order reaction model (F1) was the best common model to fit the initial and end extent of water release, α = 0.05, and 0.95. Power law (P2/3) was the best fit for α = 0.075, and 0.10 and also the next best fit for the α = 0.05. The three-dimensional diffusion (D3) model was the best fit for all αs, ranging from 0.20 to 0.80, and the next to the best fit for other models; as was expected; since the release of water from DHG was by its diffusion and vaporization through DHGs pores sites. The list-square fitting correlation was very low at the start and end of the process; it has a fair relative constancy in the range of αs 0.20 to 0.80 with the best feet to the α = 0.70 as shown in Fig. 7 (i). Moreover, judging the mechanism of dehydration by the best fitted model to the experimental data must go with the circumstances regarding to the process. Knowing that the water release mechanism involves several consecutive reactions, where the rate determining reaction is the slowest one. Also, it was assumed that the temperature dependence of the mass loss due to the water release can be described by the Arrhenius relationship, and one or more hypothetical models of the reaction mechanism, $f(\alpha)$. The kinetic triplets were determined by first selecting a rate equation and then fitting it to the experimental data. The accuracy of the results depends on the adequateness of the rate equation to describe the process. As a result, the meaningful interpretability of the determined triplets depends on whether the selected rate equation adequately captures the essential features of the process mechanism, not the precise fit to the data. In this case, the D3 model that described the sigmoidal nature of water release was the best fitting to the experimental data and the most meaningful for the process of releasing water from DHG.

The study shows that the maximum rate of water desorption depended on the heating rate. The highest rate of water generation at the heating rate, 0.5 Kmin^{-1} occurred at 48 °C, and at 5 Kmin^{-1}, it was at 107 °C, due to heat lag effects. A DSC transition was observed around 50 °C, coinciding with the maximum desorption rate of DHG observed by TGA. DSC transition confirms the release of water by DHG was facilitated by the structural transition of the DHG from a hydrophilic to a hydrophobic state.

The isoconversional method was used to construct the Arrhenius plot for a given extent of reaction (α). The results showed a relative constancy of the activation energy (Ea) within the range of 0.2 < α < 0.8, which indicated a single change, i.e., the vaporization of water during the experiment. The average values of Ea in this range were found to be 47 ± 1 kJmol^{-1}, which is comparable to the heat of vaporization of water at saturated vapor pressure. The best model to fit the experimental data was the three-dimensional diffusion model (D3).

ACKNOWLEDGEMENTS

The author acknowledges the support of the United States Department of Agriculture (USDA), National Institute of Food and Agriculture, Evans-Allen project number SCX-311-29-21. Also, we express our gratitude to Dr. J. Salley, Dr. L.

Whitesides, and their teams for their constant encouragement and support. Any opinions, findings, conclusions, or recommendations expressed in this material are those of the authors and do not necessarily reflect those of the funding agency.

COMPETING INTERESTS

Authors have declared that no competing interests exist.

REFERENCES

1. Lu H, Shi W, Zhang JH, Chen AC, Guan W, Lei C, Greer JR, Boriskina SV, Yu G. Tailoring the desorption behavior of hygroscopic gels for atmospheric water harvesting in arid climates. Advanced Materials. 2022;34:2205344. DOI:10.1002/adma.202205344
2. Graeber G, Díaz-Marín CD, Gaugler LC, Zhong Y, El Fil B, Liu X, Wang EN. Extreme water uptake of hygroscopic hydrogels through maximized swelling-induced salt loading. Advanced Materials; 2023. DOI:10.1002/adma.202211783
3. Li R, Shi Y, Alsaedi M, Wu M, Shi L, Wang P. Hybrid hydrogel with high water vapor harvesting capacity for deployable solar-driven atmospheric water generator. 2018; 52:11367–11377. DOI:10.1021/acs.est.8b02852
4. Gou X, Guo Z. Hybrid Hydrophilic-Hydrophobic CuO@TiO2-Coated Copper Mesh for Efficient Water Harvesting. Langmuir. 2020;36:64–73. DOI:10.1021/acs.langmuir.9b03224
5. Gleick PH, Cohen M, Cooley H, Donnelly K. Fulton. Julian Ha, M-L Morrison J, Phurisamban R, Rippman H, Woodward S. The world's water: The Report on Freshwater Resources; 2018;9. ISBN SBN-13.978-1983865886.
6. Meza I, Siebert S, Döll P, Kusche J, Herbert C, Eyshi Rezaei E, Nouri H, Gerdener H, Popat E, Frischen J, et al. Global-scale drought risk assessment for agricultural systems. Natural Hazards and Earth System Sciences. 2020;20:695–712. DOI:10.5194/nhess-20-695-2020
7. Boretti A, Rosa L. Reassessing the projections of the world water development report. NPJ Clean Water. 2019;2:15. DOI:10.1038/s41545-019-0039-9
8. Ciampi M. 'Water Divide' in the Global Risk Society. International Review of Sociology. 2013;23:= 243–260. DOI:10.1080/03906701.2013.771468
9. Zhou X, Lu H, Zhao F, Yu G. Atmospheric water harvesting: A review of material and structural designs; American Chemical Society. 2020;2:671–684.
10. Rubin SJ. Water costs and affordability in the United States: 1990 to 2015. J Am Water Works Assoc. 2018;110:48–52. DOI:10.1002/awwa.1062
11. Spicer N, Parlee B, Chisaakay M, Lamalice D. Drinking water consumption patterns: An Exploration of Risk Perception and Governance in Two First Nations Communities. Sustainability. 2020;12: 6851, DOI:10.3390/su12176851
12. FAO The State of the World's Land and Water Resources for Food and Agriculture – Systems at Breaking Point (SOLAW 2021); FAO; 2021. ISBN: 978-92-5-135327-1.
13. Fresán U, Marrin D, Mejia M, Sabaté J. Water footprint of meat analogs: Selected Indicators According to Life Cycle Assessment. Water (Basel). 2019;11:728. DOI:10.3390/w11040728
14. Mekonnen MM, Gerbens-Leenes W. The water footprint of global food production. Water (Basel). 2020;12:2696. DOI:10.3390/w12102696.
15. Vanham D, Mekonnen MM. The Scarcity-Weighted Water Footprint Provides Unreliable Water Sustainability Scoring. 2021;756?:143992. DOI:10.1016/j.scitotenv.2020.143992
16. Mahan D, Waissbluth O, Caceres Carcinogenic D. Non-carcinogenic health risks of arsenic exposure in drinking water in the rural environment. Global J. Environ. Sci. Manage. 2020;6:165–174.
17. Guo Y, Zhou X, Zhao F, Bae J, Rosenberger B, Yu G. Synergistic energy nanoconfinement and water activation in hydrogels for efficient solar water desalination. ACS Nano. 2019;13:7913–7919. DOI:10.1021/acsnano.9b02301
18. Xu J, Zhang J, Fu B, Song C, Shang W, Tao P, Deng T. All-day freshwater harvesting through combined solar-driven interfacial desalination and passive radiative cooling. ACS Appl Mater Interfaces. 2020;12:47612–47622. DOI:10.1021/acsami.0c14773

19. Mekonnen MM, Hoekstra AY. Four billion people facing severe water scarcity. Sci Adv. 2016;2. DOI:10.1126/sciadv.1500323
20. Pérez-González A, Urtiaga AM, Ibáñez R, Ortiz I. State of the art and review on the treatment technologies of water reverse osmosis concentrates. Water Res. 2012; 46:267–283. DOI:10.1016/j.watres.2011.10.046
21. Siddiqui MA, Azam MA, Khan MM, Iqbal S, Khan MU, Raffat Y. Current trends on extraction of water from air: An alternative solution to water supply. International Journal of Environmental Science and Technology; 2022. DOI:10.1007/s13762-022-03965-8
22. Hamidi N, Gargallo L, Whitesides L. Water and atmospheric water generation in recent progress in science and technology. In; Afefy, Prof HM, Ed, BP International (a part of Sciencedomain International). 2023; 5:43–67 ISBN 9788119102136
23. Khalil B, Adamowski J, Shabbir A, Jang C, Rojas M, Reilly K, Ozga-Zielinski B. A review: Dew water collection from radiative passive collectors to recent developments of active collectors. Sustain Water Resour Manag. 2016;2:71–86. DOI:10.1007/s40899-015-0038-z
24. Jarimi H, Powell R, Riffat S. Review of sustainable methods for atmospheric water harvesting. International Journal of Low-Carbon Technologies. 2020;15:253–276.
25. Azeem M, Noman MT, Wiener J, Petru M, Louda P. Structural design of efficient fog collectors: A review. Environ Technol Innov. 2020;20:101169. DOI:10.1016/j.eti.2020.101169
26. Zhang Y, Zhu W, Zhang C, Peoples J, Li X, Felicelli AL, Shan X, Warsinger DM, Borca-Tasciuc T, Ruan X, et al. Atmospheric water harvesting by large-scale radiative cooling cellulose-based fabric. Nano Lett. 2022;22:2618–2626. DOI:10.1021/acs.nanolett.1c04143
27. Anderson PJ, Miller AD, O'malley KA, Ceridon ML, Beck KC, Wood CM, Wiste HJ, Mueller JJ, Johnson JB, Johnson BD. Incidence and symptoms of high altitude illness in South Pole workers: Antarctic study of altitude physiology (ASAP). Clin Med Insights Circ Respir Pulm Med 2011; 5:CCRPM.S6882. DOI:10.4137/CCRPM.S6882
28. Cashman S, Ma C. (Xin), Garland J, Morelli B. Overview of resource recovery-based sustainable water systems: Life Cycle Assessment Updates from US EPA's Safe and Sustainable Water Research Program; 2018.
29. Ma X, Zhao X, Zhang Y, Liu K, Yang H, Li J, Akhlaghi YG, Liu H, Han Z, Liu Z. Combined rankine cycle and dew point cooler for energy efficient power generation of the power plants - A review and perspective study. Energy. 2022;238: 121688. DOI:10.1016/j.energy.2021.121688
30. Park H, Haechler I, Schnoering G, Ponte M.D, Schutzius TM, Poulikakos D. Enhanced atmospheric water harvesting with sunlight-activated sorption ratcheting. ACS Appl Mater Interfaces. 2022;14: 2237–2245. DOI:10.1021/acsami.1c18852
31. Xi Z, Li S, Yu L, Yan H, Chen M. All-day freshwater harvesting by selective solar absorption and radiative cooling. ACS Appl Mater Interfaces. 2022;14:26255–26263. DOI:10.1021/acsami.2c05409
32. Liu X, Beysens D, Bourouina T. Water harvesting from air: Current Passive Approaches and Outlook; American Chemical Society. 2022;4:1003–1024.
33. Kim S, Choi H. Switchable wettability of thermoresponsive core–shell nanofibers for water capture and release. ACS Sustain Chem Eng. 2019;7:19870–19879. DOI:10.1021/acssuschemeng.9b05273
34. Diouf D, Darmanin T, Diouf A, Dieng SY, Guittard F. Surface nanostructuration and wettability of electrodeposited poly(3,4-Ethylenedioxypyrrole) and Poly(3,4-Propylenedioxypyrrole) films substituted by aromatic groups. ACS Omega. 2018;3: L8393–8400. DOI:10.1021/acsomega.8b00871
35. Thakur N, Sargur Ranganath A, Sopiha K, Baji A. Thermoresponsive cellulose acetate-poly(N-Isopropylacrylamide) core-shell fibers for controlled capture and release of moisture. ACS Appl Mater Interfaces. 2017;9:29224–29233. DOI:10.1021/acsami.7b07559
36. Echeverria C, Fernandes S, Godinho M, Borges J, Soares P. Functional stimuli-responsive gels: Hydrogels and Microgels. Gels. 2018;4:54. DOI:10.3390/gels4020054
37. Hamidi N, Zhu T. Characterization of amphiphilic cobaltocenium copolymers via

size exclusion chromatography with online laser-light scattering and viscometric detectors. Journal of Macromolecular Science, Part B. 2021;60:30–50. DOI:10.1080/00222348.2020.1819600
38. Wei M, Gao Y, Li X, Serpe MJ. Stimuli-responsive polymers and their applications. Polym Chem. 2017;8:127–143. DOI:10.1039/C6PY01585A
39. Guo Y, Bae J, Fang Z, Li P, Zhao F, Yu G. Hydrogels and hydrogel-derived materials for energy and water sustainability. Chem Rev. 2020;120:7642–7707.
40. Hanikel N, Prévot MS, Yaghi OM. MOF water harvesters. Nat Nanotechnol. 2020; 15:348–355. DOI:10.1038/s41565-020-0673-x
41. Nguyen HL, Gropp C, Hanikel N, Möckel A, Lund A, Yaghi OM. Hydrazine-hydrazide-linked covalent organic frameworks for water harvesting. ACS Cent Sci; 2022. DOI:10.1021/acscentsci.2c00398
42. Kallenberger PA, Fröba M. Water harvesting from air with a hygroscopic salt in a hydrogel–derived matrix. Commun Chem. 2018;1:28. DOI:10.1038/s42004-018-0028-9
43. Yilmaz G, Meng FL, Lu W, Abed J, Peh CKN, Gao M, Sargent EH, Ho GW. Autonomous atmospheric water seeping MOF matrix. Sci Adv. 2020;6. DOI:10.1126/sciadv.abc8605
44. Zhao F, Zhou X, Liu Y, Shi Y, Dai Y, Yu G. Super moisture-absorbent gels for all-weather atmospheric water harvesting. Advanced Materials. 2019;31:1806446. DOI:10.1002/adma.201806446
45. Díaz-Marín CD, Zhang L, Lu Z, Alshrah M, Grossman JC, Wang EN. Kinetics of sorption in hygroscopic hydrogels. Nano Lett. 2022;22:1100–1107. DOI:10.1021/acs.nanolett.1c04216
46. Flory PJ. Principles of Polymer Chemistry; Cornell University Press: Ithaca, NY; 1953.
47. Bertrand T, Peixinho J, Mukhopadhyay S, MacMinn CW. Dynamics of swelling and drying in a spherical Gel. Phys Rev Appl. 2016;6:064010. DOI:10.1103/PhysRevApplied.6.064010
48. LaPotin A, Kim H, Rao SR, Wang EN. Adsorption-based atmospheric water harvesting: Impact of material and component properties on system-level performance. Acc Chem Res. 2019;52: 1588–1597. DOI:10.1021/acs.accounts.9b00062
49. Gid, B, Friedler E, Broday DM. Liquid-desiccant vapor separation reduces the energy requirements of atmospheric moisture harvesting. Environ Sci Technol. 2016;50:8362–8367. DOI:10.1021/acs.est.6b01280
50. Mulchandani A, Edberg J, Herckes P, Westerhoff P. Seasonal atmospheric water harvesting yield and water quality using electric-powered desiccant and compressor dehumidifiers. Science of The Total Environment. 2022;825:153966. DOI:10.1016/j.scitotenv.2022.153966
51. Mehta JR, Desai TK, Patel AK, Diyora HB, Rabadiya AS. Preliminary investigations on a novel rotating media liquid-air contacting device without liquid pool. In Proceedings of the Energy Procedia; Elsevier Ltd. March 1 2017;109:167–173.
52. Entezari A, Ejeian M, Wang R. Super atmospheric water harvesting hydrogel with alginate chains modified with binary salts. ACS Mater Lett. 2020;2:471–477. DOI:10.1021/acsmaterialslett.9b00315
53. Liu X, Wang X, Kapteijn F. Water and metal-organic frameworks: From interaction toward utilization. Chem Rev 2020;120:8303–8377.
54. Feng R, Xu, C, Song F, Wang F, Wang X.-L.L, Wang Y.-Z.Z. A bioinspired slippery surface with stable lubricant impregnation for efficient water harvesting. 2020;12: 12373–12381. DOI:10.1021/acsami.0c00234
55. Zhu S-Q, Feng R, Liang Z-H, Wang X-L, Wang Y-Z, Song F. Efficient water harvesting enabled by porous architecture-containing hybrid surfaces. Ind Eng Chem Res; 2022. DOI:10.1021/acs.iecr.2c00717
56. Aleid S, Wu M, Li R, Wang W, Zhang C, Zhang L, Wang P. Salting-in effect of zwitterionic polymer hydrogel facilitates atmospheric water harvesting. ACS Mater Lett. 2022;4:511–520. DOI:10.1021/acsmaterialslett.1c00723
57. Pérez-Maqueda LA, Criado JM, Sánchez-Jiménez PE. Combined kinetic analysis of solid-state reactions: A Powerful tool for the simultaneous determination of kinetic parameters and the kinetic model without previous assumptions on the reaction mechanism. J Phys Chem A. 2006;110: 12456–12462. DOI:10.1021/jp064792g

58. Hamidi N. Upcycling Poly(Vinyl Chloride) waste tubes: Studies of thermal stability and kinetics of films made of waste polyvinylchloride tube at the initial steps of degradation. J Appl Polym Sci. 2023;140. DOI:10.1002/app.53663
59. Hamidi N, Yazdani-Pedram M, Abdussalam N. Upcycling Poly(Ethylene Terephthalate) wastes by solvent extraction: thermal stability and kinetics Studies of the Recovered <scp>PET</Scp>. J Appl Polym Sci. 2022; 139:51905. DOI:10.1002/app.51905
60. Vyazovkin S, Burnham AK, Favergeon L, Koga N, Moukhina E, Pérez-Maqueda L.A., Sbirrazzuoli N. ICTAC kinetics committee recommendations for analysis of multi-step kinetics. Thermochim Acta. 2020;689:178597. DOI:10.1016/j.tca.2020.178597
61. Peterson JD, Vyazovkin S, Wight CA. Kinetics of the thermal and thermo-oxidative degradation of polystyrene, polyethylene and poly(Propylene); 2001; 202.
62. Dong Z, Yang Y, Cai W, He Y, Chai M, Liu B, Yu X, Banks SW, Zhang X, Bridgwater AV et al. Theoretical analysis of double logistic distributed activation energy model for thermal decomposition kinetics of solid fuels. Ind Eng Chem Res. 2018;57:7817–7825. DOI:10.1021/acs.iecr.8b01527
63. Atkin P, De Paula, J. Physical Chemistry, 9th Edition; W. H. Freeman, 2009: New York, NY; 2009;9.
64. Sbirrazzuoli N. Advanced Isoconversional kinetic analysis for the elucidation of complex reaction mechanisms: A New Method for the Identification of Rate-Limiting Steps. Molecules. 2019;24:1683. DOI:10.3390/molecules24091683
65. Ding J, Zhang X, Hu D, Ye S, Jiang J. Model-free kinetic determination of pre-exponential factor and reaction mechanism in accelerating rate calorimetry. thermochim acta. 2021;702:178983. DOI:10.1016/j.tca.2021.178983
66. Sbirrazzuoli N. Determination of pre-exponential factors and of the mathematical functions f(α) or G(α) that describe the reaction mechanism in a Model-Free Way. Thermochim Acta. 2013; 564:59–69. DOI:10.1016/j.tca.2013.04.015

Peer-review history:
The peer review history for this paper can be accessed here:
https://www.sdiarticle5.com/review-history/105081